HHS Public Access

Author manuscript

Angiogenesis. Author manuscript; available in PMC 2015 June 21.

Published in final edited form as:

Angiogenesis. 2012 September ; 15(3): 433–442. doi:10.1007/s10456-012-9271-3.

Quantitative assessment of tumor angiogenesis using real-time motion-compensated contrast-enhanced ultrasound imaging

Marybeth A. Pysz,
Molecular Imaging Program at Stanford, Department of Radiology, Stanford University School of Medicine, 300 Pasteur Drive, Room H1307, Stanford, CA, USA

Ismayil Guracar,
Siemens Healthcare, Ultrasound Business Unit, Mountain View, CA, USA

Kira Foygel,
Molecular Imaging Program at Stanford, Department of Radiology, Stanford University School of Medicine, 300 Pasteur Drive, Room H1307, Stanford, CA, USA

Lu Tian, and
Department of Health, Research and Policy, Stanford University, Stanford, CA, USA

Jürgen K. Willmann
Molecular Imaging Program at Stanford, Department of Radiology, Stanford University School of Medicine, 300 Pasteur Drive, Room H1307, Stanford, CA, USA

Abstract

Purpose—To develop and test a real-time motion compensation algorithm for contrast-enhanced ultrasound imaging of tumor angiogenesis on a clinical ultrasound system.

Materials and methods—The Administrative Institutional Panel on Laboratory Animal Care approved all experiments. A new motion correction algorithm measuring the sum of absolute differences in pixel displacements within a designated tracking box was implemented in a clinical ultrasound machine. In vivo angiogenesis measurements (expressed as percent contrast area) with and without motion compensated maximum intensity persistence (MIP) ultrasound imaging were analyzed in human colon cancer xenografts (n = 64) in mice. Differences in MIP ultrasound imaging signal with and without motion compensation were compared and correlated with displacements in x- and y-directions. The algorithm was tested in an additional twelve colon cancer xenograft-bearing mice with (n = 6) and without (n = 6) anti-vascular therapy (ASA-404). In vivo MIP percent contrast area measurements were quantitatively correlated with ex vivo microvessel density (MVD) analysis.

Results—MIP percent contrast area was significantly different ($P < 0.001$) with and without motion compensation. Differences in percent contrast area correlated significantly ($P < 0.001$) with x- and y-displacements. MIP percent contrast area measurements were more reproducible

J. K. Willmann willmann@stanford.edu.

Electronic supplementary material The online version of this article (doi:10.1007/s10456-012-9271-3) contains supplementary material, which is available to authorized users.

with motion compensation (ICC = 0.69) than without (ICC = 0.51) on two consecutive ultrasound scans. Following anti-vascular therapy, motion-compensated MIP percent contrast area significantly (P = 0.03) decreased by 39.4 ± 14.6 % compared to non-treated mice and correlated well with ex vivo MVD analysis (Rho = 0.70; P = 0.05).

Conclusion—Real-time motion-compensated MIP ultrasound imaging allows reliable and accurate quantification and monitoring of angiogenesis in tumors exposed to breathing-induced motion artifacts.

Keywords

Maximum intensity persistence; MIP; Cancer; Ultrasound; Microbubbles; Vascular disrupting agent; VDA

Introduction

Contrast-enhanced ultrasound imaging with contrast microbubbles (gas-filled, lipid-shelled microspheres) is increasingly being used for detection and characterization of diseases in the abdomen and pelvis [1–18], heart [19–21], breast [22–24], head and neck [25, 26], and brain [27]. In addition to detection and characterization of diseases by analyzing enhancement patterns following contrast micro-bubble administration, contrast-enhanced ultrasound allows quantification of angiogenesis which could be used for stratifying and monitoring cancer patients undergoing new anti-angiogenic or anti-vascular therapy [2, 28, 29]. Various techniques for quantification of angiogenesis can be used in contrast-enhanced ultrasound imaging, including the analysis of time-intensity curves after microbubble bolus injection [28, 30], assessment of tissue reperfusion after microbubble destruction and replenishment during continuous infusion of microbubbles [31–36], or measurement of maximum intensity persistence (MIP) imaging plateau values [30, 37, 38].

In MIP ultrasound imaging, the image frames are summed over time resulting in the visual outline of blood vessels as microbubbles trace through; as a result, visual maps of tissue vascularity are obtained in real-time following microbubble bolus administration [3, 30, 37]. Recent studies have shown that MIP ultrasound imaging allows reliable and accurate quantification and monitoring of tumor angiogenesis during anti-angiogenic therapy, using ex vivo analyses as reference standard [30, 37]. Furthermore, it has been shown that quantification of tumor angiogenesis with MIP ultrasound imaging is less dependent on the contrast injection rate compared with traditional time-intensity analysis approaches [30], suggesting that MIP ultrasound imaging may become a robust and promising real-time tool for tumor angiogenesis quantification in the clinic [30]. However, a major challenge of quantitative MIP ultrasound imaging is the frequent technical failure due to motion artifacts [3], and motion compensation techniques are critically needed to improve this technique and to help translating this promising approach into the clinic [3].

Therefore, the purpose of our study was to develop and implement a novel real-time motion compensation algorithm for a clinical ultrasound imaging system, and to test this algorithm for MIP ultrasound imaging in human colon cancer xenografts with breathing-induced

motion artifacts and in mice undergoing anti-vascular therapy with a vascular disruptive agent.

Materials and methods

Human colon cancer xenografts in mice

Experimental procedures on laboratory animals were approved by the Institutional Administrative Panel on Laboratory Animal Care. Human LS174T colon adeno-carcinoma cells (ATCC; Manassas, VA) were cultured in Minimum Essential Medium supplemented with 10 % fetal bovine serum, and grown to 70–80 % confluency prior to trypsinization and preparation for injection. 3×10^6 cells were resuspended in 50 μl of Matrigel (BD Biosciences, San Jose, CA), and then injected subcutaneously on the mid-back region of 76 6–8 weeks old, female nude mice (Charles River, Wilmington, MA). This anatomical region was chosen since breathing motion-artifacts in murine subcutaneous tumor xenografts are pronounced at the level of the thorax. Tumors were grown for 5–12 days to obtain a broad spectrum of tumor volumes. Tumor volumes were calculated by using the formula for a prolate ellipsoid ($\pi/6 \times$ length $\times$ width $\times$ height, as measured by ultrasound) and averaged 867 ± 547 mm^3 (range 187–2,600 mm^3).

Contrast-enhanced ultrasound imaging settings

Human colon cancer xenografts were imaged with a Siemens Sequoia Acuson 512 clinical ultrasound scanner equipped with a prototype motion compensation software, and a 15L8 linear array transducer (Siemens Medical Solutions, Mountain View, CA) at a center frequency of 10.5 MHz (bandwidth, 65 %) and a mechanical index of 0.26. Brightness (B)-mode and contrast-enhanced images, acquired using contrast-pulse sequencing (CPS), were displayed side-by-side. The transducer was aligned to the center of the tumor (gauged by largest diameter), and images were zoomed to a 20 mm (x-direction) by 15 mm (y-direction) field-of-view. An acoustic focus zone was placed at the level of the tumor, and time/gain compensation was applied to provide background tissue noise minimization (the gain was kept constant at −20 in all animals). After the above machine settings were established for the first animal, the same settings were applied for all animals in all experiments by aligning the tumor in the fixed field of view. Contrast-enhanced images were acquired in the MIP mode, which records the maximum intensity obtained on a pixel by pixel analysis over all acquired imaging frames, thereby creating a visual map of the tumor vasculature [30, 37, 39]. A region of interest (ROI) was drawn manually over all tumors before contrast agent administration, and MIP percent contrast area as a measure of percent tumor vascular perfusion within the ROI was calculated in real-time after the contrast reached equilibrium in the blood (represented as the imaging plateau value of the MIP percent contrast area curve; Fig. 1) [30, 37, 39]. The MIP percent contrast area was calculated as the percentage of pixels above the user-defined threshold intensity (threshold = 70 on scale from 0 (black) to 255 (white) out of all the pixels contained within the ROI (Fig. 1). In all mice, 5×10^7 (180 μl injection volume) perfluorobutane-containing contrast microbubbles (Micro-markers™; Visual Sonics, Toronto, Canada) were injected intravenously via a tail vein catheter at a constant injection rate of 1.2 ml/min using an infusion pump (Genie Plus; Kent Scientific, Torrington, CT), and real-time MIP percent contrast area measurements both with

and without motion compensation were collected as described below. To assess reproducibility, MIP percent contrast area measurements with and without motion compensation were repeated 24 h apart in a subgroup of 6 mice.

Design of motion compensation algorithm

A prototype motion compensation algorithm (see Supplementary Material) was developed and integrated into the software of a Sequoia Acuson 512 (Siemens; Mountain View, CA) clinical ultrasound system. A rectangular user-defined motion tracking box was implemented with adjustable size (width and height) and location (depth and lateral location) (Fig. 1). During scanning, this tracking box was placed over the tumor on the B-mode images. Real-time motion compensation was accomplished by measurement of the vertical and horizontal displacements within the tracking box, and minimal displacements within the tracking box were searched by the technique of sum of absolute differences (SAD) [40], according to the following equation:

$$SAD_{u,v}=\sum_{j=1}^{M}\sum_{k=1}^{N}\left|I_{reference}\left(j,k\right)-I_{tracked}\left(j+u,k+v\right)\right| \quad (1)$$

where the rectangular tracking box size is $M \times N$ pixels and the displacement search region over u and v is 16 × 16 samples, corresponding to a maximum displacement of 0.75 mm in vertical (y) and 1.0 mm in lateral (x) directions. The sampling indices, j and k, are used to sum the absolute value of the difference between the reference image and the tracked image over the region of interest. The reference frame, $I_{reference}$ is the first tracking portion of the first B-mode frame in the capture sequence. The tracked frame, $I_{tracked}$ is the tracking portion of the current B-mode frame to be input to the MIP algorithm.

The best fit horizontal and vertical displacement region of interest being tracked was then applied to the entire current frame in both B-mode and contrast mode in real-time during data acquisition in MIP mode. If a large motion-induced displacement was detected during the capture interval [a large displacement was defined as a displacement greater than 5 % of the image width or height; at our settings, 5 % of 15 mm was 0.75 mm (y-direction); and 5 % of 20 mm was 1.0 mm (x-direction)], the MIP data acquisition was temporarily gated off to “protect” the MIP data acquisition from transient large displacement events. During these gated off intervals, the color of the tracking box was changed from green to red to indicate that tracking was not being maintained.

Contrast-enhanced MIP ultrasound imaging data collection with and without motion compensation

To allow an intra-animal comparison of MIP ultrasound imaging data acquired in the same anatomical location and during the same contrast agent bolus injection both with and without motion compensation in the first group of 64 mice, non-motion-compensated and motion-compensated MIP percent coverage area data and corresponding images were simultaneously recorded in the system memory, and access to these data in memory was implemented through a toggle switch on the ultrasound machine. After the MIP percent contrast area reached plateau following contrast agent administration as described above,

motion-compensated MIP mode data collection was stopped, and the motion-compensated MIP image frames were stored on the ultrasound machine. The display was then toggled to the non-motion compensated MIP mode data collection, and the non-compensated MIP image frames were stored on the ultrasound machine. MIP percent contrast area and displacements in x- and y-directions over time were recorded as text files in addition to JPEG-format images.

MIP ultrasound imaging data analysis

Motion-induced displacement data were imported into Microsoft Excel and analyzed in random order by one blinded reader. Minimum, maximum, average, and standard deviations of motion-induced direction-independent [absolute values of x: to the left (positive values) or right (negative values); y: upwards (positive values) or downwards (negative values)] displacements in tumor ROIs were calculated. Differences between MIP percent contrast area without motion compensation and the MIP percent contrast area with motion compensation (MIP percent contrast area$|_{\text{MC OFF}}$ − MIP percent contrast area$|_{\text{MC ON}}$) were also calculated.

Motion-compensated MIP ultrasound imaging for monitoring anti-vascular therapy

In an additional group of 12 animals with human colon cancer xenografts, a baseline contrast-enhanced MIP ultrasound imaging scan was acquired as detailed above. Mice were then randomly divided into 2 groups: Mice in group 1 (n = 6) were treated with a single intravenous administration of a vascular disruptive agent (ASA404; 15 mg/kg; Novartis, Basel, Switzerland; 55 μl), and mice in the control group 2 (n = 6) received a single intravenous injection of 55 μl saline only. Twenty-four hours after treatment, all tumors were re-scanned in approximately the same imaging plane using the same protocol as described above with and without real-time motion compensation.

Ex vivo analysis of tumors with immunofluorescence

After ultrasound imaging, tumors were excised and frozen in Optimum Cutting Temperature (OCT; Tissue-Tek®, Fisher Scientific, Pittsburgh, PA). Frozen tissues sections (10 μm; 1 section per tumor) were mounted on microscope slides for immunofluorescence staining. The sections were fixed in ice-cold acetone and immunostained for vascular endothelial cells overnight at 4 degree Celsius with 1:100 primary rat anti-mouse CD31 antibody (Abcam, Inc., Cambridge, MA). Secondary antibody [donkey anti-rat FITC-conjugated antibody (Jackson Immunoresearch, West Grove, PA)] was applied at 1:300 dilution in phosphate-buffered saline (Invitrogen, Carlsbad, CA) for 30 min at room temperature. Coverslips were then mounted onto slides with anti-fading medium (Fisher Scientific, Pittsburgh, PA). Fluorescent micrographs (100×) were captured using a microscope (Axiovert 25; Carl Zeiss, Thornwood, NY) and a digital camera (AxioCam, Bernried, Germany). Microvessel density analysis of non-treated (n = 5) and treated (n = 5) was performed by summing the total number of vessels in 7 fields of view (per section), and averaging per total field of view area (micrograph area was 0.14 μm^2) for each tissue section [41].

Statistical analysis

All values were expressed as mean ± SD. Two sample comparisons were analyzed using the nonparametric Wilcoxon rank test. Paired comparisons were analyzed using the one-sample Wilcoxon rank test. Correlation data were analyzed by calculation of the correlation coefficient (between two contiguous measures) and the corresponding 95 % confidence interval (CI) based on Fisher's transformation. Interclass correlation coefficient (ICC) was estimated for evaluating agreement between two consecutive measurements and the 95 % CI for ICC were constructed with the bootstrap method. ICCs were defined as follows: ICC, 0–0.20: no agreement; ICC, 0.21–0.40: poor agreement; ICC, 0.41–0.60: moderate agreement; ICC, 0.61–0.80: good agreement; and ICC, > 0.80: excellent agreement [42]. All statistical analyses were performed using R.2.10.1 software (http://www.r-project.org/). A P value < 0.05 was considered statistically significant.

Results

Effect of motion compensation on quantification of tumor angiogenesis

In order to assess the ability to compensate for motion artifacts during the real-time quantification of vascular perfusion with ultrasound MIP imaging, the difference in percent contrast area between images acquired with and without motion compensation was calculated. Overall, there was a significant difference ($P < 0.001$) in measured MIP percent contrast area with and without motion compensation in human colon cancer xenografts (mean difference 9.7 ± 8.1 %; range 0.5–33.3 %) (Fig. 2a). A deep breath (gasping) occurred in 28 of 64 (44 %) mice during MIP ultrasound imaging data acquisition, whereas there was no gasping in 36/64 mice (56 %). Mean difference on motion-compensated versus non-compensated MIP images regarding measured percent contrast area in mice with gasping was 14.9 ± 8.2 % (range 2.3–33.3 %) (Fig. 2b, c); this was significantly higher ($P < 0.001$) compared to the difference in percent contrast area in mice without gasping (mean 5.7 ± 5.2 %; range 0.5–18.8 %). Deep breathing occurred randomly in mice and was observed at the beginning, mid period and end of MIP ultrasound imaging data acquisition.

Measurement of motion-induced displacements within the B-mode tracking box ranged from 0.0 to 1.6 mm (mean 0.3 ± 0.3 mm) in the x-direction and from 0.1 to 1.6 mm (mean 0.7 ± 0.4 mm) in the y-direction (Fig. 2d). Displacements in the y-direction were notably higher than displacements in the x-direction (Fig. 2d), which is partly due to the position of the tumor on the back of the mice (also see Supplementary videos). Displacements both in x-direction (Rho = 0.56, 95 % CI: 0.37, 0.71; $P < 0.001$) and y-direction (Rho = 0.68; 95 % CI: 0.53, 0.80; $P < 0.001$) significantly correlated with differences in MIP percent contrast area between motion-compensated and non-compensated MIP ultrasound images. These data indicate that significantly more motion artifacts occurred with larger displacements, and the real-time motion compensation algorithm could reliably correct for instances such as a deep breath.

Reproducibility of motion-compensated MIP ultrasound imaging of tumor angiogenesis

Measurements of MIP percent contrast areas at two consecutive days with motion correction were reproducible (ICC = 0.69; 95 % CI: 0.34, 0.93). Reproducibility of MIP percent

contrast area measurements was decreased without motion compensation (ICC = 0.51; 95 % CI: 0.12, 0.89) (Fig. 3).

Monitoring anti-vascular therapy with motion-compensated MIP ultrasound imaging and correlation with ex vivo analysis

There was no significant difference (P = 1.00) in tumor volumes before treatment administration between mice with (896 ± 576 mm^3; range 462–2,039 mm^3) versus without (925 ± 592 mm^3; range 420–2,039 mm^3) vascular disruptive therapy. Twenty-four hours following anti-vascular therapy, percent contrast area significantly (P = 0.03) decreased from an average 55.7 ± 13.3 % (range 44.2–75.6 %) to an average 16.3 ± 11.8 % (range 5.7–39.3 %) (Fig. 4). In contrast, in saline-treated control mice, percent contrast area did not significantly change (P = 1.00) after 24 h (mean percent contrast area before treatment, 63.0 ± 12.1 %; range 49.7–84.4 %; after saline treatment, 60.6 ± 21.5 %; range 37.5–95.0 %). After treatment, microvessel density significantly (P < 0.03) decreased in treated mice (12.9 ± 9.3 vessels per μm^2) compared to non-treated control mice (31.5 ± 4.9 vessels per μm^2) (Fig. 4). In vivo MIP percent contrast areas correlated well with ex vivo measurement of tumor angiogenesis (Rho = 0.70; P = 0.05). Tumor volumes did not change in treated mice (P = 0.3) and increased (P = 0.01) in saline-treated control mice after 24 h.

Discussion

Our results showed that real-time motion compensation during contrast-enhanced MIP ultrasound imaging is feasible for accurate and reliable quantification of tumor angiogenesis in a human colon cancer xenograft model exposed to motion. In vivo motion-compensated MIP percent contrast areas correlated well in assessing and monitoring extent of tumor angiogenesis compared to ex vivo analysis during anti-vascular therapy. The new motion compensation algorithm may further facilitate establishment of contrast-enhanced ultrasound imaging as a reliable and accurate tool for real-time quantification of tumor angiogenesis both in preclinical and clinical applications.

Due to its advantages including broad availability, versatility and portability, relatively low costs, and lack of irradiation exposure, contrast-enhanced ultrasound imaging has increasingly been explored for clinical management of patients (e.g., with focal liver lesions among several other indications) [1, 43–45]. In addition to the option of analyzing enhancement patterns in real-time over several minutes following intravenous contrast microbubble injection with improved detection and tissue characterization of for example tumors compared to non-enhanced B-mode imaging, contrast-enhanced ultrasound allows assessment of tumor perfusion and angiogenesis [1]. Since ultrasound contrast agents can also be modified to attach to molecular markers of angiogenesis [46, 47], thereby shedding some light on the molecular profile of developing and treated tumors [48, 49], contrast-enhanced ultrasound has a great potential as a non-invasive imaging tool for functional and molecular monitoring of angiogenesis during tumor growth and following treatments such as anti-angiogenic and anti-vascular therapies in the clinic [2, 47, 50–52]. However, since ultrasound is a real-time exam with often active inclusion of the patient into the work flow of the examination, contrast-enhanced ultrasound can be hampered by motion artifacts,

including motion from patient movement and breathing artifacts. In a recent study of 17 patients with renal cell carcinoma undergoing anti-angiogenic therapy with sunitinib, respiratory motion caused substantial errors in quantifying vascular properties of tumors assessed both with the technique of bolus time-intensity analysis and disruption-replenishment with often large fluctuations in the time-intensity curves [52]. Similarly, in a study of 65 patients with focal liver lesions undergoing MIP ultrasound imaging, inability to suspend respiration with consecutive motion artifacts was the most common reason for failed ultrasound MIP ultrasound imaging [3]. Ultrasound MIP imaging quantifies tumor angiogenesis with a technique analogous to “photographing a moving light at night with a long exposure” [3]. It is, therefore, particularly prone to motion-induced artifacts [3, 30].

In our study we developed a new real-time motion-compensation algorithm for a clinical ultrasound system and tested this technique for ultrasound MIP imaging in a human colon cancer xenograft mouse model. To maximize respiratory motion-induced artifacts in this mouse model, human xenografts were implanted onto the back of mice to simulate colon cancer metastases to an organ exposed to motion, such as the liver. Also, gasping of some mice under anesthesia with a single deep breath in our study simulated a clinical situation with patients unable to hold the breath with short deep breathing in between breath holdings. Our study showed that quantitative ultrasound MIP imaging data were substantially affected by respiratory motion induced artifacts and that motion compensation resulted in significant differences up to 33.3 % in the estimation of tumor angiogenesis compared to non-corrected images. Not surprisingly, these differences in measured tumor angiogenesis with and without motion correction were most pronounced in mice that spontaneously gasped during data acquisition. Although spontaneous gasping was not a standardized respiratory excursion with mice taking differently deep inspirations at different time points of data acquisition, it was a helpful model to simulate more pronounced motion artifacts compared to the relatively small excursions from regular breathing in mice. Although we could not influence the occurrence of gasping in mice it was observed in a substantial 44 % of ultrasound exams in our study.

To also assess reproducibility of motion-compensated MIP ultrasound imaging, a subgroup of mice were scanned two times, 24 h apart. We found that motion-compensated MIP ultrasound imaging was reproducible with an ICC of 0.69, while reproducibility was smaller without motion compensation (interclass coefficient of 0.51). Our findings confirm results from a recent study that demonstrated high reliability of MIP ultrasound imaging at consecutive imaging sessions in a mouse hind limb tumor model that was not affected by motion [37].

Preclinical MIP ultrasound imaging has also previously been used to measure vascular changes following cancer treatment with anti-angiogenic therapies. Anti-vascular endothelial growth factor (VEGF) antibody therapy (B20-4.1.1; Genentech) resulted in moderate decreases (mean: 25 %) in vascularity measured with MIP ultrasound imaging 48 h post-treatment [37]. In contrast, the small molecule receptor tyrosine kinase inhibitor, SU11248 (Sutent; Pfizer) more drastically reduced (mean: 43 %) MIP ultrasound signal after 24 h of treatment, and continued to have reducing effects on MIP signal at 48 and 96 h post-treatment [30]. Since MIP ultrasound imaging may also be useful for evaluating other

agents for inhibiting tumor blood supply, we tested motion-compensated MIP ultrasound imaging for monitoring tumor angiogenesis following vascular disruptive therapy (ASA404; Novartis). In vivo MIP percent contrast area substantially decreased 24 h after intravenous administration of ASA404 while MIP percent contrast area did not significantly change in saline-treated control mice. Notably, there was no significant change in tumor volumes in treated mice after 24 h. Ex vivo analysis of tumors after treatment confirmed a significant decrease in microvessel density with no significant changes in control mice. Furthermore, in vivo imaging signal correlated well with ex vivo microvessel density, suggesting that motion-compensated MIP ultrasound imaging allows non-invasive monitoring of tumor angiogenesis in anatomical regions affected by motion artifacts.

In previous studies, real-time motion compensation have been accomplished using respiratory gating [53, 54] or registration-based [55] approaches; however, these techniques require the use of additional monitoring equipment (e.g., respiration monitoring electrodes or radiofrequency) to co-register with the ultrasound scanning system [56], and can decrease the temporal resolution of ultrasound data acquisition [53, 54, 57]. Our proposed motion-correction algorithm is a simple and robust technique that allows motion compensation in real time using the SAD method on B-mode images which is an easy-to-compute approach with small computational time and without the need of additional equipment. This real-time motion tracking algorithm was also applied to measure rat kidney perfusion dynamics (analyzing microbubble arrival time) following vasodilation or vasoconstriction [58]. In our study, we further improve this software to increase the flexibility of tracking with a size- and location-adjustable tracking box. We also validate for the first time that the real-time motion compensation algorithm results in accurate measurements of tumor angiogenesis using MIP ultrasound imaging and we show that quantitative motion-corrected values are significantly different compared to measurements without motion compensation.

We acknowledge several limitations of our study. First, the new real-time motion compensation algorithm allowed correction of motion artifacts only for in-plane motion in the x and y directions and could not correct for out-of-plane motion artifacts. However, our animal model was focused on simulating breathing-induced artifacts by placing the tumor onto the back of the mice with the majority of displacements in the y direction (up/down), and was not intended to account for out-of-plane motion (e.g., occurring when there is spontaneous movement of the entire body of the animal, which we did not observe with the animals under anesthesia during ultrasound scanning). Furthermore, while in this proof-of-principle study, we only tested the effects of motion compensation for ultrasound MIP imaging, it is likely that other quantitative contrast-enhanced ultrasound approaches such as time-intensity analysis, destruction-replenishment methods, and ultrasound molecular imaging may benefit from this technique and prospective experiments are needed to test this hypothesis. Finally, we did not implant the human colon cancer xenografts orthotopically into the liver which may have better reflected the anatomical environment of colon metastases to the liver. However, we chose to instead implant the tumors at the back of the mice because we found it technically less challenging to reliably localize subcutaneously implanted xenografts versus orthotopic liver xenografts using a clinical ultrasound transducer at a 10.5 MHz center frequency, considering the small anatomical dimensions in

mice. Also, for longitudinal imaging experiments, we could better localize the approximate same imaging plane in subcutaneous versus orthotopic xenografts.

In conclusion, our results suggest that ultrasound MIP imaging combined with a new motion compensation algorithm allows reliable and accurate real-time quantification and monitoring of tumor angiogenesis in a mouse tumor model with breathing-induced motion artifacts. Future developments are needed to scale this technique from small animals to humans to further establish quantitative contrast-enhanced ultrasound imaging for angiogenesis imaging in the clinical arena.

Supplementary Material

Refer to Web version on PubMed Central for supplementary material.

Acknowledgments

We would like to acknowledge the support by the NIH R21 CA139279 grant, the NCI ICMIC CA114747 P50 developmental grant, the SMIS NIH fellowship program, and the Canary Foundation. We also acknowledge Novartis (Basel, Switzerland) for provision of the ASA-404 VDA therapy, and Siemens for provision of the clinical ultrasound machine.

References

1. Wilson SR, Burns PN. Microbubble-enhanced US in body imaging: what role? Radiology. 2010; 257:24–39. [PubMed: 20851938]
2. Lassau N, Chami L, Chebil M, Benatsou B, Bidault S, Girard E, Abboud G, Roche A. Dynamic contrast-enhanced ultra-sonography (DCE-US) and anti-angiogenic treatments. Discov Med. 2011; 11:18–24. [PubMed: 21276407]
3. Wilson SR, Jang HJ, Kim TK, Iijima H, Kamiyama N, Burns PN. Real-time temporal maximum-intensity-projection imaging of hepatic lesions with contrast-enhanced sonography. AJR Am J Roentgenol. 2008; 190:691–695. [PubMed: 18287440]
4. Aigner F, Mitterberger M, Rehder P, Pallwein L, Junker D, Horninger W, Frauscher F. Status of transrectal ultrasound imaging of the prostate. J Endourol. 2010; 24:685–691. [PubMed: 20433367]
5. Aigner F, Pallwein L, Mitterberger M, Pinggera GM, Mikuz G, Horninger W, Frauscher F. Contrast-enhanced ultrasonography using cadence-contrast pulse sequencing technology for targeted biopsy of the prostate. BJU Int. 2009; 103:458–463. [PubMed: 19021610]
6. DePriest PD, DeSimone CP. Ultrasound screening for the early detection of ovarian cancer. J Clin Oncol. 2003; 21:194s–199s. [PubMed: 12743134]
7. Fleischer AC, Lyshchik A, Andreotti RF, Hwang M, Jones HW III, Fishman DA. Advances in sonographic detection of ovarian cancer: depiction of tumor neovascularity with micro-bubbles. AJR Am J Roentgenol. 2010; 194:343–348. [PubMed: 20093594]
8. Fleischer AC, Lyshchik A, Jones HW III, Crispens MA, Andreotti RF, Williams PK, Fishman DA. Diagnostic parameters to differentiate benign from malignant ovarian masses with contrast-enhanced transvaginal sonography. J Ultrasound Med. 2009; 28:1273–1280. [PubMed: 19778872]
9. Gorg C. The forgotten organ: contrast enhanced sonography of the spleen. Eur J Radiol. 2007; 64:189–201. [PubMed: 17920224]
10. Fusaroli P, Spada A, Mancino MG, Caletti G. Contrast harmonic echo-endoscopic ultrasound improves accuracy in diagnosis of solid pancreatic masses. Clin Gastroenterol Hepatol. 2010; 8(629–634):e621–e622.
11. Helmstaedter L, Riemann JF. Pancreatic cancer—EUS and early diagnosis. Langenbecks Arch Surg. 2008; 393:923–927. [PubMed: 18247044]

12. Hohl C, Schmidt T, Honnef D, Gunther RW, Haage P. Ultrasonography of the pancreas. 2. Harmonic imaging. Abdom Imaging. 2007; 32:150–160. [PubMed: 16850350]
13. Rickes S, Rauh P, Uhle C, Ensberg D, Monkemuller K, Malfertheiner P. Contrast-enhanced sonography in pancreatic diseases. Eur J Radiol. 2007; 64:183–188. [PubMed: 17869470]
14. Correas JM, Claudon M, Tranquart F, Helenon AO. The kidney: imaging with microbubble contrast agents. Ultrasound Q. 2006; 22:53–66. [PubMed: 16641794]
15. Xu ZF, Xu HX, Xie XY, Liu GJ, Zheng YL, Lu MD. Renal cell carcinoma and renal angiomyolipoma: differential diagnosis with real-time contrast-enhanced ultrasonography. J Ultrasound Med. 2010; 29:709–717. [PubMed: 20427782]
16. Doust BD. The use of ultrasound in the diagnosis of gastroenterological disease. Gastroenterology. 1976; 70:602–610. [PubMed: 767196]
17. Nylund K, Hausken T, Gilja OH. Ultrasound and inflammatory bowel disease. Ultrasound Q. 2010; 26:3–15. [PubMed: 20216190]
18. Nylund K, Odegaard S, Hausken T, Folvik G, Lied GA, Viola I, Hauser H, Gilja OH. Sonography of the small intestine. World J Gastroenterol. 2009; 15:1319–1330. [PubMed: 19294761]
19. Contamin H, Rioufol G, Bettinger T, Helbert A, Portier KG, Lepage OM, Thomas R, Broillet A, Tranquart F, Schneider M. A minimally-invasive closed chest myocardial occlusion-reperfusion model in rhesus monkeys (Macaca mulatta): monitoring by contrast-enhanced ultrasound imaging. Int J Cardiovasc Imaging. 2012; 28:531–542. [PubMed: 21484234]
20. Staub D, Partovi S, Schinkel AF, Coll B, Uthoff H, Aschwanden M, Jaeger KA, Feinstein SB. Correlation of carotid artery atherosclerotic lesion echogenicity and severity at standard US with intraplaque neovascularization detected at contrast-enhanced US. Radiology. 2011; 258:618–626. [PubMed: 20971776]
21. Staub D, Schinkel AF, Coll B, Coli S, van der Steen AF, Reed JD, Krueger C, Thomenius KE, Adam D, Sijbrands EJ, ten Cate FJ, Feinstein SB. Contrast-enhanced ultrasound imaging of the vasa vasorum: from early atherosclerosis to the identification of unstable plaques. JACC Cardiovasc Imaging. 2010; 3:761–771. [PubMed: 20633855]
22. Balleyguier C, Opolon P, Mathieu MC, Athanasiou A, Garbay JR, Delaloge S, Dromain C. New potential and applications of contrast-enhanced ultrasound of the breast: Own investigations and review of the literature. Eur J Radiol. 2009; 69:14–23. [PubMed: 18977102]
23. Caproni N, Marchisio F, Pecchi A, Canossi B, Battista R, D'Alimonte P, Torricelli P. Contrast-enhanced ultrasound in the characterisation of breast masses: utility of quantitative analysis in comparison with MRI. Eur Radiol. 2010; 20:1384–1395. [PubMed: 20033178]
24. Hooley RJ, Andrejeva L, Scoutt LM. Breast cancer screening and problem solving using mammography, ultrasound, and magnetic resonance imaging. Ultrasound Q. 2011; 27:23–47. [PubMed: 21343800]
25. Molinari F, Mantovani A, Deandrea M, Limone P, Garberoglio R, Suri JS. Characterization of single thyroid nodules by contrast-enhanced 3-D ultrasound. Ultrasound Med Biol. 2010; 36:1616–1625. [PubMed: 20800947]
26. Zengel P, Siedek V, Berghaus A, Clevert DA. Intraductally applied contrast-enhanced ultrasound (IA-CEUS) for improved visualization of obstructive diseases of the salivary glands, primary results. Clin Hemorheol Microcirc. 2010; 45:193–205. [PubMed: 20675900]
27. de Lange C, Brabrand K, Emblem KE, Bjornerud A, Loberg EM, Saugstad OD, Munkeby BH. Cerebral perfusion in perinatal hypoxia and resuscitation assessed by transcranial contrast-enhanced ultrasound and 3 T MRI in newborn pigs. Invest Radiol. 2011; 46:686–696. [PubMed: 21730873]
28. Lamuraglia M, Bridal SL, Santin M, Izzi G, Rixe O, Paradiso A, Lucidarme O. Clinical relevance of contrast-enhanced ultrasound in monitoring anti-angiogenic therapy of cancer: current status and perspectives. Crit Rev Oncol Hematol. 2010; 73:202–212. [PubMed: 19546008]
29. Yoshida K, Hirokawa T, Moriyasu F, Liu L, Liu GJ, Yamada M, Imai Y. Arterial-phase contrast-enhanced ultrasonography for evaluating anti-angiogenesis treatment: a pilot study. World J Gastroenterol. 2010; 17:1045–1050. [PubMed: 21448357]
30. Palmowski M, Lederle W, Gaetjens J, Socher M, Hauff P, Bzyl J, Semmler W, Gunther RW, Kiessling F. Comparison of conventional time-intensity curves vs. maximum intensity over time

for post-processing of dynamic contrast-enhanced ultrasound. Eur J Radiol. 2010; 75:e149–e153. [PubMed: 19945241]

31. Hoyt K, Warram JM, Umphrey H, Belt L, Lockhart ME, Robbin ML, Zinn KR. Determination of breast cancer response to bevacizumab therapy using contrast-enhanced ultrasound and artificial neural networks. J Ultrasound Med. 2010; 29:577–585. [PubMed: 20375376]
32. Pollard RE, Sadlowski AR, Bloch SH, Murray L, Wisner ER, Griffey S, Ferrara KW. Contrast-assisted destruction-replenishment ultrasound for the assessment of tumor microvasculature in a rat model. Technol Cancer Res Treat. 2002; 1:459–470. [PubMed: 12625773]
33. Watson KD, Hu X, Lai CY, Lindfors HA, Hu-Lowe DD, Tuthill TA, Shalinsky DR, Ferrara KW. Novel ultrasound and DCE-MRI analyses after antiangiogenic treatment with a selective VEGF receptor inhibitor. Ultrasound Med Biol. 2011; 37:909–921. [PubMed: 21531499]
34. Zhou JH, Cao LH, Liu JB, Zheng W, Liu M, Luo RZ, Han F, Li AH. Quantitative assessment of tumor blood flow in mice after treatment with different doses of an antiangiogenic agent with contrast-enhanced destruction-replenishment US. Radiology. 2011; 259:406–413. [PubMed: 21292869]
35. Arditi M, Frinking PJ, Zhou X, Rognin NG. A new formalism for the quantification of tissue perfusion by the destruction-replenishment method in contrast ultrasound imaging. IEEE Trans Ultrason Ferroelectr Freq Control. 2006; 53:1118–1129. [PubMed: 16846144]
36. Wei K, Jayaweera AR, Firoozan S, Linka A, Skyba DM, Kaul S. Quantification of myocardial blood flow with ultrasound-induced destruction of microbubbles administered as a constant venous infusion. Circulation. 1998; 97:473–483. [PubMed: 9490243]
37. Pysz MA, Foygel K, Panje CM, Needles A, Tian L, Willmann JK. Assessment and monitoring tumor vascularity with contrast-enhanced ultrasound maximum intensity persistence imaging. Invest Radiol. 2011; 46:187–195. [PubMed: 21150790]
38. Zhao H, Xu R, Ouyang Q, Chen L, Dong B, Huihua Y. Contrast-enhanced ultrasound is helpful in the differentiation of malignant and benign breast lesions. Eur J Radiol. 2010; 73:288–293. [PubMed: 19559551]
39. Dave JK, Forsberg F. Novel automated motion compensation technique for producing cumulative maximum intensity subharmonic images. Ultrasound Med Biol. 2009; 35:1555–1563. [PubMed: 19616359]
40. Bohs LN, Trahey GE. A novel method for angle independent ultrasonic imaging of blood flow and tissue motion. IEEE Trans Biomed Eng. 1991; 38:280–286. [PubMed: 2066142]
41. Weidner N. Chapter 14. Measuring intratumoral micro-vessel density. Methods Enzymol. 2008; 444:305–323. [PubMed: 19007671]
42. Faria JR, Aarao AR, Jimenez LM, Silva OH, Avelleira JC. Inter-rater concordance study of the PASI (Psoriasis Area and Severity Index). An Bras Dermatol. 2010; 85:625–629. [PubMed: 21152786]
43. Dindyal S, Kyriakides C. Ultrasound microbubble contrast and current clinical applications. Recent Pat Cardiovasc Drug Discov. 2011; 6:27–41. [PubMed: 21222650]
44. McCarville MB. Contrast-enhanced sonography in pediatrics. Pediatr Radiol. 2011; 41(Suppl 1):S238–S242. [PubMed: 21523607]
45. Xu HX. Contrast-enhanced ultrasound: the evolving applications. World J Radiol. 2009; 1:15–24. [PubMed: 21160717]
46. Pochon S, Tardy I, Bussat P, Bettinger T, Brochot J, von Wronski M, Passantino L, Schneider M. BR55: a lipopeptide-based VEGFR2-targeted ultrasound contrast agent for molecular imaging of angiogenesis. Invest Radiol. 2010; 45:89–95. [PubMed: 20027118]
47. Pysz MA, Foygel K, Rosenberg J, Gambhir SS, Schneider M, Willmann JK. Antiangiogenic cancer therapy: monitoring with molecular US and a clinically translatable contrast agent (BR55). Radiology. 2010; 256:519–527. [PubMed: 20515975]
48. Palmowski M, Huppert J, Ladewig G, Hauff P, Reinhardt M, Mueller MM, Woenne EC, Jenne JW, Maurer M, Kauffmann GW, Semmler W, Kiessling F. Molecular profiling of angiogenesis with targeted ultrasound imaging: early assessment of antiangiogenic therapy effects. Mol Cancer Ther. 2008; 7:101–109. [PubMed: 18202013]

49. Deshpande N, Ren Y, Foygel K, Rosenberg J, Willmann JK. Tumor angiogenic marker expression levels during tumor growth: longitudinal assessment with molecularly targeted microbubbles and US imaging. Radiology. 2011; 258:804–811. [PubMed: 21339349]
50. Lassau N, Koscielny S, Chami L, Chebil M, Benatsou B, Roche A, Ducreux M, Malka D, Boige V. Advanced hepatocellular carcinoma: early evaluation of response to bevacizumab therapy at dynamic contrast-enhanced US with quantification—preliminary results. Radiology. 2011; 258:291–300. [PubMed: 20980447]
51. Lavisse S, Lejeune P, Rouffiac V, Elie N, Bribes E, Demers B, Vrignaud P, Bissery MC, Brule A, Koscielny S, Peronneau P, Lassau N. Early quantitative evaluation of a tumor vasculature disruptive agent AVE8062 using dynamic contrast-enhanced ultrasonography. Invest Radiol. 2008; 43:100–111. [PubMed: 18197062]
52. Williams R, Hudson JM, Lloyd BA, Sureshkumar AR, Lueck G, Milot L, Atri M, Bjarnason GA, Burns PN. Dynamic microbubble contrast-enhanced US to measure tumor response to targeted therapy: a proposed clinical protocol with results from renal cell carcinoma patients receiving antiangiogenic therapy. Radiology. 2011; 260:581–590. [PubMed: 21555352]
53. Averkiou M, Lampaskis M, Kyriakopoulou K, Skarlos D, Klouvas G, Strouthos C, Leen E. Quantification of tumor microvascularity with respiratory gated contrast enhanced ultrasound for monitoring therapy. Ultrasound Med Biol. 2010; 36:68–77. [PubMed: 19900749]
54. Mule S, De Cesare A, Frouin F, Lucidarme O, Herment A. An original methodology for quantitative assessment of perfusion in small animal studies using contrast-enhanced ultrasound. Conf Proc IEEE Eng Med Biol Soc. 2007; 2007:347–350. [PubMed: 18001961]
55. Frangi AF, Laclaustra M, Lamata P. A registration-based approach to quantify flow-mediated dilation (FMD) of the brachial artery in ultrasound image sequences. IEEE Trans Med Imaging. 2003; 22:1458–1469. [PubMed: 14606679]
56. de Oliveira PL, de Senneville BD, Dragonu I, Moonen CT. Rapid motion correction in MR-guided high-intensity focused ultrasound heating using real-time ultrasound echo information. NMR Biomed. 2010; 23:1103–1108. [PubMed: 20669159]
57. Mule S, Kachenoura N, Lucidarme O, De Oliveira A, Pellot-Barakat C, Herment A, Frouin F. An automatic respiratory gating method for the improvement of microcirculation evaluation: application to contrast-enhanced ultrasound studies of focal liver lesions. Phys Med Biol. 2011; 56:5153–5165. [PubMed: 21775793]
58. Pollard RE, Dayton PA, Watson KD, Hu X, Guracar IM, Ferrara KW. Motion corrected cadence CPS ultrasound for quantifying response to vasoactive drugs in a rat kidney model. Urology. 2009; 74:675–681. [PubMed: 19589583]

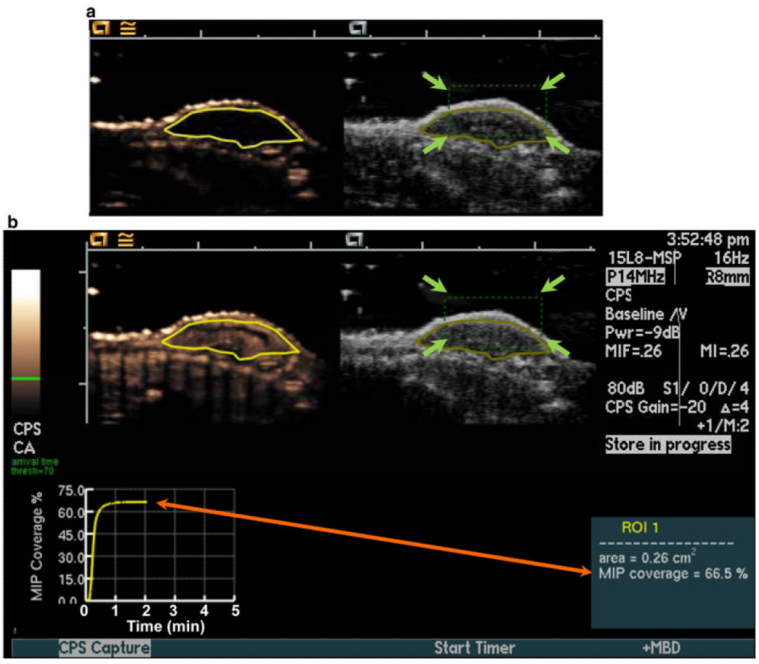

Fig. 1.

Setup for real-time maximum intensity persistence (MIP) ultrasound imaging with motion compensation. Motion compensation was accomplished by manually placing a tracking box (*green dotted line; green arrows*) over the subcutaneous human colon cancer xenografts located on the back of mice (**a**). A region of interest (ROI; *yellow outline of tumor*) was drawn on both contrast mode (*left*) and B-mode (*right*) images before contrast agent injection for real-time measurement of MIP percent contrast area. **b** MIP percent contrast area in the ROI was calculated in real-time after contrast reached equilibrium and was displayed graphically on the ultrasound screen (*orange arrow*). (Color figure online)

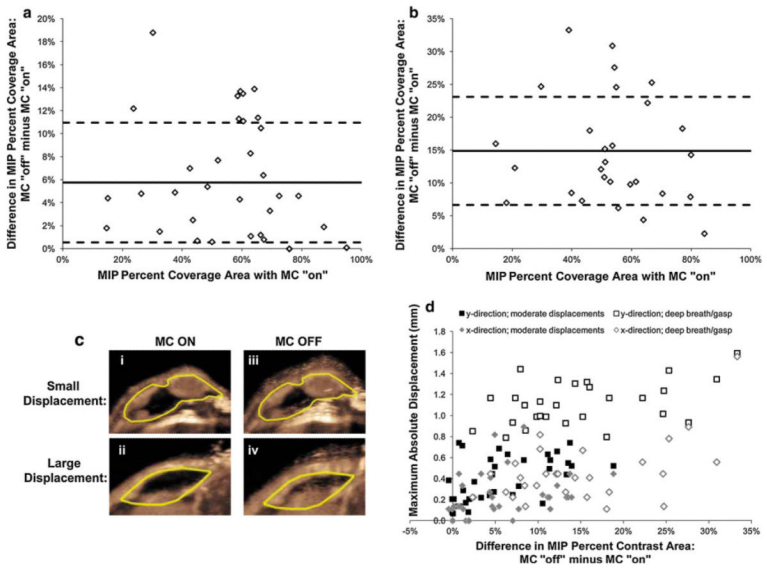

Fig. 2.

Differences in MIP percent coverage area between vascular measurements with and without motion compensation (y-axis: subtraction of motion compensation (MC) OFF minus MC ON) for individual animals with varying vascularity levels (*x*-axis: motion-compensated MIP percent coverage area); **a** summary of data in animals with moderate breathing artifacts; **b** summary of animals where a deep breath or gasp occurred. *Solid lines* represent the average value and *dashed lines* are the standard deviation for all individuals on each *plot*. **c** Representative transverse US images of two human colon cancer xenografts (*yellow line*, ROI) show intra-animal comparisons of MIP percent contrast areas measured with (*MC ON; i and ii*) and without (*MC OFF; iii* and *iv*) motion compensation (MC) in an animal with moderate breathing artifacts (*small displacement*) and in an animal where a deep breath/gasp occurred (*large displacement*). Note that varying levels of motion-induced blurring artifacts occur without motion compensation (*MC OFF*) compared with motion compensation (*MC ON*), especially when larger motion was a result of a deep breath (*large displacement*). **d** Individual displacements in both *x*- and *y-directions* significantly correlated well ($P < 0.001$) with differences measured between motion compensated and non-compensated MIP signal (Difference = MC OFF minus MC ON). (Color figure online)

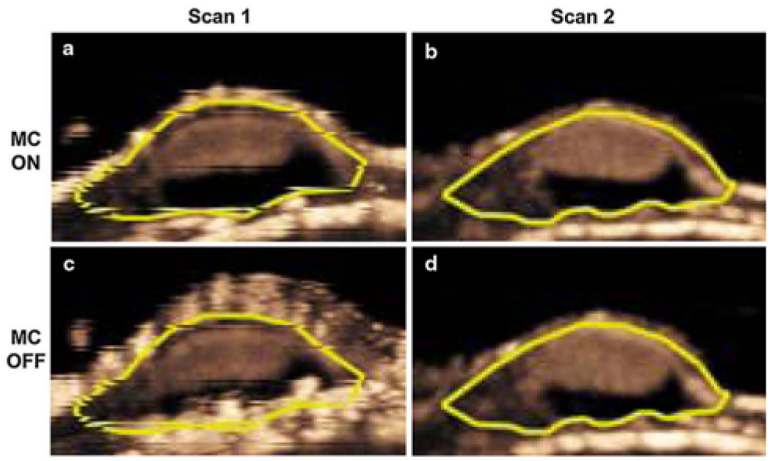

Fig. 3.

Transverse MIP ultrasound images of a representative human colon cancer xenograft scanned twice (separated by 24 h) with (**a, b**) and without (**c, d**) motion compensation (MC). Note that measured MIP percent contrast area was more reproducible on the two consecutive scans when motion compensation was turned on (*MC on*) compared to non-compensated (*MC off*) images. Also note that the mouse gasped during the first exam, resulting in substantial motion-induced blurring artifacts on non-compensated image (**c**)

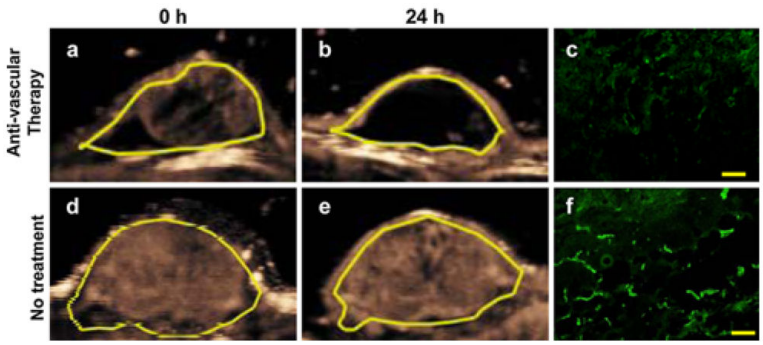

Fig. 4.

Representative two consecutive (24 h apart) transverse MIP ultrasound images of a human colon cancer xenograft in a mouse with (**a, b**) and in another mouse without (**d, e**) anti-vascular therapy using a vascular disruptive agent. Note substantial decrease in measured MIP percent contrast area in treated xenograft and no significant change of MIP percent contrast area in non-treated xenograft. Ex vivo microvessel density analysis confirmed decreased angiogenesis in treated (**c**) xenograft and no significant change in non-treated xenograft (**f**). *Yellow scale* in **c** and **f** = 100 μm. (Color figure online)